Int. J. Heat Mass Transfer. Vol. 13, pp. 145–159. Pergamon Press 1970. Printed in Great Britain

ANALYTICAL INVESTIGATION OF HEAT OR MASS TRANSFER AND FRICTION FACTORS IN A CORRUGATED DUCT HEAT OR MASS EXCHANGER

D. F. SHERONY* and C. W. SOLBRIG†

Illinois Institute of Technology

(*Received* 26 *August* 1968 *and in revised form* 14 *May* 1969)

Abstract—Heat and mass transfer design parameters are readily available for flow in circular and flat ducts for a variety of boundary conditions. However, the boundaries of the flow passages found in regenerators, rotary heat exchangers, rotary mass exchangers, etc. are usually, of necessity, other than circular or parallel plate. One very common exchanger made up of many flow passages looks like the end view of several layers of corrugated cardboard. The boundary of the cross-section normal to the flow of one of these passages may be represented by a sine curve from $-\pi$ to π forming the upper portion of the duct and a flat plate stretched between $-\pi$ and π to form the bottom portion of the boundary.

This paper presents the computed friction factors and Nusselt numbers (or Sherwood numbers) of this geometry for several aspect ratios and Biot numbers (or wall reaction rates). These results agree well with the very limited experimental data reported in the literature. Since the data in the literature are limited, this analysis provides additional design information on a very important heat and mass transfer geometry. The results obtained could not be adequately estimated from the results of a circular geometry or a flat duct because the corners in the sinusoidal duct provide an inherently different geometry. The results also differ considerably from a triangular duct. An unusual result for the sinusoidal geometry is the behaviour of the Nusselt number. It decreases with decreasing Biot Number.

NOMENCLATURE

a, half duct height as shown in Fig. 1;
A, area of duct;
b, quarter duct width as shown in Fig. 1;
Bi, wall Biot number, $Bi = 2ah_w/k$;
C_p, heat capacity;
C, concentration;
$\overline{C}$, dimensionless concentration;
D, diffusivity;
D_h, hydraulic diameter, $D_h = 4A/\overline{P}$;
E_T, truncation error;
f, dimensionless velocity $f = u_z\mu/(\mathrm{d}p/\mathrm{d}z)(4a^2)$;
F, friction factor defined by equation (8);
g, dimensionless velocity, u_z/U;
h_w, wall heat transfer coefficient, constant;
k, thermal conductivity;
k_w, wall reaction rate constant;
K, constant defined by equation (11);
K_w, dimensionless wall reaction rate;
N_{Pe}, Peclet number, $N_{Pe} = N_{Re} \cdot N_{Pr}$;
N_{Pr}, Prandtl number;
N_{Re}, Reynolds number, $D_hU\rho/\mu$;
N_{Sh}, Sherwood number, k_wD_h/D;
Nu_z, local Nusselt number defined by equation (33);
Nu_{oz}, local Nusselt number defined by equation (36);
p, pressure;
$\overline{P}$, wetted perimeter;
R, $\Delta\zeta/(\Delta\eta)^2$, $\Delta\zeta/(\Delta\xi)^2$;
t, time;
T, temperature;
T_i, initial temperature;

* Department of Chemical Engineering, Illinois Institute of Technology.

† Department of Gas Engineering, IIT, and the Institute of Gas Technology.

T_w, wall temperature;
$\bar{T}$, dimensionless temperature defined by equation (21);
u_z, velocity component in z direction;
U, average velocity in z direction;
x, coordinate as defined in Fig. 2;
y, coordinate as defined in Fig. 2;
z, coordinate as defined in Fig. 2;
Z_e, hydrodynamic entrance length;
α_i, coefficients defined by equation (57);
γ, aspect ratio, a/b;
ζ, dimensionless length, $zD_h/4a^2N_{Pe}$;
η, dimensionless coordinate, $\eta = y/2a$;
λ, angle defined in Fig. 3;
μ, viscosity;
ξ, dimensionless coordinate, $\xi = x/2b$;
ρ, density;
τ, dimensionless time;
τ, wall shear stress.

INTRODUCTION

THE CORRUGATED duct geometry is quite common in rotary heat and mass exchangers and is becoming more so. The geometry is advantageous because of its simplicity of construction and large surface area. A limited amount of experimental measurements of heat transfer coefficients have been published [1]. No analytical studies have previously been made on this geometry. Because of the nature of the flow passages as well as the small size of the passages, it is very difficult to measure anything but overall unsteady state measurements. Because of the dearth of experimental data, the analytical solution of this problem is important and supplies much needed design information.

The corrugated duct geometry is illustrated in Fig. 1. The flow is normal to the page. It is observed that a single tube may be approximated quite accurately with a sine curve for one portion of the boundary and a flat plate on the remaining part. This geometry is inherently different than most geometries which have been studied analytically including the triangular duct. The reason is the shape of the corners which provide very high flow resistance and poor heat transfer. The zero angle of contact produces a much larger stagnant volume than for triangular passages. The local heat or mass transfer coefficient becomes very small in the corners, thus causing a much lower overall coefficient [1].

The primary methods which could be used to solve this problem are:

1. Completely analytical solutions.
2. Variational methods which rely upon using satisfactory trial functions.
3. Finite difference techniques.

The first is useful to prove that Nusselt numbers approach a constant for large values of the flow direction. A finite difference technique has been used here to obtain the numerical results.

The unsteady state problem has been reduced to a steady state problem in the initial time period. The solution of heat or mass transfer problem is a Graetz type problem and produces Nusselt numbers which can be used in overall studies of the unsteady state problem such as the ones performed by Locke [2] and Schumann [3]. These later studies assume that the heat transfer coefficient is known. The analysis presented here determines it. The effects of peripheral and axial conduction in the solid have been neglected here and are probably negligible in the mass transfer problems considered here. In the heat transfer problem, the axial conduction effect is negligible for certain regions of flow, duct size, and material as indicated by an overall study [1, 4, 5]. The effect of peripheral conduction is also negligible in certain instances depending upon the material and its thickness. This effect may be estimated from a study performed for a rectangular channel [6]. The heat or mass transfer in the normal direction in the wall has been assumed infinite. This is a good assumption for heat transfer but may be important in certain mass transfer problems.

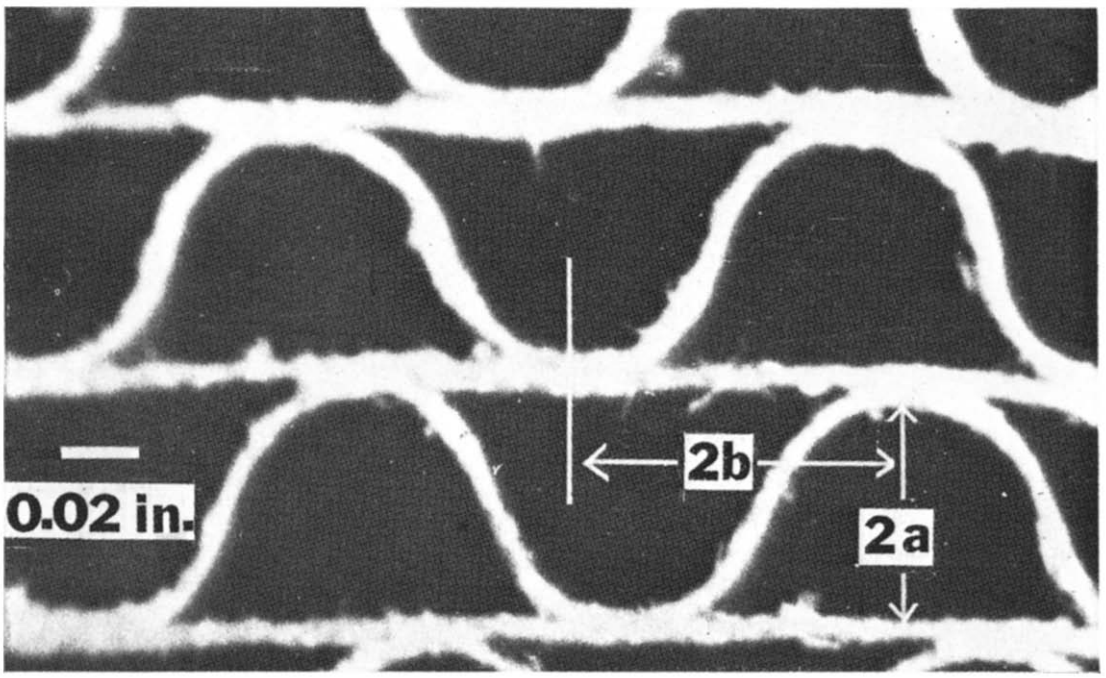

FIG. 1. Corrugated configuration.

[*facing page* 146]

FORMULATION OF EQUATIONS

Velocity profile

All the assumptions normally made in a Graetz problem will be used here [7, 8]. The velocity profile will be assumed independent of the heat or mass transfer processes occurring. The fluid and flow matrix properties are assumed constant. Density changes due to temperature and concentration variations, therefore, will be neglected. This is a good assumption for many heat exchangers as well as chemical reactors with small changes in the number of moles and a small heat of reaction and is particularly good for the sorption of water as in a rotary dehumidifier. The momentum entrance length will be assumed small and only the fully developed profile will be calculated.

The flow geometry is indicated in Fig. 2. Since the flow is independent of the unsteady

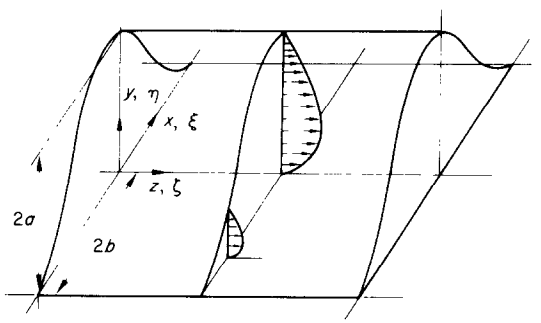

FIG. 2. Flow geometry.

state heat or mass transfer problem, all unsteady state terms in the continuity and momentum equations may be neglected. Since the flow is fully developed, u_x and u_y are zero. With these assumptions, the continuity equation becomes,

$$\frac{\partial u_z}{\partial z} = 0. \tag{1}$$

The x, y and z momentum equations utilizing the above assumptions and equation (1) becomes respectively,

$$\frac{\partial p}{\partial x} = 0 \tag{2}$$

$$\frac{\partial p}{\partial y} = 0 \tag{3}$$

$$\mu\left(\frac{\partial^2 u_z}{\partial x^2} + \frac{\partial^2 u_z}{\partial y^2}\right) = \frac{\partial p}{\partial z}. \tag{4}$$

Equations (1)–(4) imply that $\partial p/\partial z$ is a constant.

Let $y = 2a \cdot \eta$, $x = 2b \cdot \xi$

$$f(\xi, \eta) = \frac{u_z \mu}{(-\mathrm{d}p/\mathrm{d}z)(2a)^2}$$

so that equation (4) becomes

$$\gamma^2 \frac{\partial^2 f}{\partial \xi^2} + \frac{\partial^2 f}{\partial \eta^2} = -1. \tag{5}$$

The dimensionless velocity is related to the average velocity U and f by the relation

$$\frac{u_z}{U} = \frac{f(\xi, \eta)}{\iint f \,\mathrm{d}\xi \,\mathrm{d}\eta} = g(\xi, \eta) \tag{6}$$

where $\iint$ indicates integration over the region bounded by $\eta = 0$, and $\eta = 1 + \cos \pi\xi$.

The average velocity is

$$U = \frac{(-\mathrm{d}p/\mathrm{d}z)(2a)^2}{\mu} \cdot \iint f \,\mathrm{d}\xi \,\mathrm{d}\eta \tag{7}$$

The friction factor F may be determined from equation (7) and the usual definitions

$$-\frac{\mathrm{d}p}{\mathrm{d}z} = \frac{\overline{P}}{A} \cdot \tau$$

$$\tau = \frac{F}{4} \rho \frac{U^2}{2}$$

where τ is the average wall shear stress, $\overline{P}$ is the perimeter, and A is the area. The friction factor may be solved for as

$$F = \frac{2\left[\dfrac{2}{\displaystyle\int_{-1}^{1} \left\{1 + \left(\frac{\pi}{2}\gamma \sin \pi\xi\right)^2\right\}^{\frac{1}{2}} \mathrm{d}\xi}\right]^2}{[N_{Re} \cdot \iint f \,\mathrm{d}\xi \,\mathrm{d}\eta]}. \tag{8}$$

As usual in laminar flow, $F \cdot N_{Re}$ is independent of the flow rate. The pressure drop in the

entrance region as well as the hydrodynamic entrance length can be estimated from the work of McComas [9]. The pressure drop in the entrance region is

$$P_0 - P_e = \tfrac{1}{2}\rho U^2 \left(F\frac{Z_e}{D_h} + K\right). \tag{9}$$

The entrance length, Z_e, is given by

$$\frac{Z_e}{D_h N_{Re}} = \frac{(U_m/U)^2 - 1 - K}{C} \tag{10}$$

where U_m is the maximum velocity.

C is from equation (8) in the form $F = C/N_{Re}$ and

$$K = 2\iint\left[\left(\frac{u_z}{U}\right)^3 - \left(\frac{u_z}{U}\right)^2\right]\mathrm{d}\xi\,\mathrm{d}\eta \tag{11}$$

The relation between the dimension a and the hydraulic diameter is

$$\frac{D_h}{2a} = \frac{2}{1 + \int_0^1 \left[1 + \left(\frac{\pi}{2}\gamma \sin \pi\xi\right)^2\right]^{\frac{1}{2}} \mathrm{d}\xi} \tag{12}$$

A HEAT TRANSFER PROBLEM

The usual experimental steady state technique of measuring heat transfer coefficients in a single tube cannot be used for the geometry under consideration [2]. In a single tube, a fluid with a large thermal capacity may be circulated on the outside of the tube to maintain the surface temperature of the tube constant. One of the principal advantages of the sinusoidal duct is the fact that it fills the entire space when combined with other tubes of the same geometry. However, the fact that it does exist in a matrix prohibits the above steady state experiment. Therefore, an unsteady state experiment must be performed. Locke [2] discussed many different experimental methods of determining the heat transfer coefficient. Howard [1] has performed a very accurate experiment. The temperature of the matrix is brought to a uniform temperature by passing a gas of uniform temperature through it for a sufficient amount of time. The matrix is then moved quickly to a stream parallel to the first but at a different temperature by means of a sliding mechanism. This experiment closely describes the actual operation of a rotary heat or mass exchanger where different portions of the exchanger are exposed to different streams.

The equations which describe the temperatures are:

In the gas phase

$$\rho C_p \frac{\partial T}{\partial z} + \rho C_p u_z \frac{\partial T}{\partial z} = k\left(\frac{\partial^2 T}{\partial x^2} + \frac{\partial^2 T}{\partial y^2} + \frac{\partial^2 T}{\partial z^2}\right). \tag{13}$$

Where viscous dissipation has been neglected and fully developed flow is assumed. Calculated values of the momentum entrance length are presented in the results section. The incoming temperature of the gas is

$$T(t, x, y, 0) = T_i \tag{14}$$

In the solid phase

$$\rho_s C_{ps} \frac{\partial T_s}{\partial t} = k_s \nabla^2 T_s \tag{15}$$

$$T_s(0, x, y, z) = T_{si}. \tag{16}$$

The heat flux across the layer between the gas and solid phase is:

$$-k\frac{\partial T}{\partial n} = h_w[T(\text{interface}) - T_s(\text{interface})] = -k_s\frac{\partial T_s}{\partial n} \tag{17}$$

where n is the normal at the surface.

A layer which produces an effective resistance between the fluid and solid is assumed to exist to take into account the possibility of fouling by a thin layer of stagnant fluid such as oil or deposition of a crud in the exchanger. Substitution of dimensionless quantities into equation (13) yields

$$N_{Pr} \cdot \frac{\rho}{\mu} \frac{(2a)^2}{\tau_0} \frac{\partial T}{\partial t'} + g(\xi, \eta) \frac{\partial T}{\partial \zeta} = \left[\gamma^2 \frac{\partial^2 T}{\partial \xi^2} + \frac{\partial^2 T}{\partial \eta^2} + \left(\frac{D_h}{N_{Pe} \cdot 2a} \right)^2 \frac{\partial^2 T}{\partial \zeta^2} \right]$$

where

$$t' = \frac{t}{\tau_0} \quad \text{and} \quad \tau_0 = \text{a characteristic time.}$$

$$\zeta = \frac{z}{N_{Pe} \cdot D_h (2a/D_h)^2}$$

$N_{Pe} = N_{Re} \cdot N_{Pr}$.

The characteristic time of measurement is at least on the order of one second, and using τ_0 equal to one second produces a value of 10^{-4} for the coefficient of $\partial T/\partial t'$.

For Peclet numbers from 10 to 100, the coefficient of $\partial^2 T/\partial \zeta^2$ varies from 10^{-2} to 10^{-4}. Since the coefficients of these terms are extremely small, these terms may be dropped to yield the equation

$$g(\xi, \eta) \frac{\partial T}{\partial \zeta} = \gamma^2 \frac{\partial^2 T}{\partial \xi^2} + \frac{\partial^2 T}{\partial \eta^2} \tag{18}$$

with the initial condition

$$T(\xi, \eta, 0) = T_i. \tag{19}$$

Because of the large thermal inertia of the solid relative to gas, the temperature of the solid may be assumed constant during the initial transient period so that equations (15)–(17) may be replaced with

$$-k \left. \frac{\partial T}{\partial n} \right|_w = h_w (T_w - T_{si}) = \frac{k_w}{\delta} (T_w - T_{si}), \tag{20}$$

where w indicates the layer between gas and solid and δ indicates the thickness of this layer and is assumed constant. The solution of equations (18)–(20) can yield results which will relate the mixing cup inlet and outlet temperatures to, N_{Pe}, γ, and the wall Biot number, $2a \cdot k_w/\delta \cdot k$. Although the outlet temperature is a function of time, the required value at $t = 0$ can be obtained by extrapolation.

In terms of the dimensionless temperature,

$$\overline{T} = \frac{T - T_{si}}{T_i - T_{si}}. \tag{21}$$

Equations (18)–(20) become

$$g(\xi, \eta) \frac{\partial \overline{T}}{\partial \zeta} = \gamma^2 \frac{\partial^2 \overline{T}}{\partial \xi} + \frac{\partial^2 \overline{T}}{\partial \eta^2} \tag{22}$$

$$\overline{T}(\xi, \eta, 0) = 1 \tag{23}$$

$$- \left. \frac{\partial \overline{T}}{\partial \overline{n}} \right|_w = Bi \overline{T}|_w \tag{24}$$

where

$$\overline{n} = \frac{n}{2a}.$$

MASS TRANSFER—A CATALYTIC REACTOR

The mass conversion in a catalytic reactor may be described by equations (22)–(24) if the reaction rate is described in terms of one component

$$D \frac{\partial C}{\partial n} = k_w \cdot C, \tag{25}$$

where the equation of species is to be written in terms of mass units—since the mass of the system is constant [8]. This problem may be described by replacing $\overline{C} = C/C_i$ in equations (22) and (23), where C_i is the initial mass fraction, and replacing equation (24) by

$$\frac{\partial \overline{C}}{\partial \overline{n}} = K_w \overline{C} \tag{26}$$

where

$$K_w = \frac{k_w \cdot 2a}{D},$$

the dimensionless wall reaction rate.

MASS TRANSFER—SORPTION

The sorption of water on a salt is an unsteady state problem. However, the estimates and

consequent simplification of the transfer equation apply to transfer of water from the gas phase to the solid. Although the total mass of the system is not constant, the difference between the inlet and outlet mass flow rate cannot be changed by more than one per cent due to the loss of water vapor. Thus, the velocity may be described by equation (4). The boundary condition, when using the diluteness assumption, may be expressed as

$$-D\frac{\partial C}{\partial n} = k_w(C - C_{eq}) \tag{27}$$

where C_{α} is the equilibrium mass concentration in terms of the vapor pressure in equilibrium with the hydrate. The equilibrium vapor pressure at constant temperature is independent of the concentration in the solid (unless a new hydrate is formed) so that C_{eq} is independent of time. If $\overline{C}$ is defined as

$$\overline{C} = \frac{C - C_{eq}}{C_i - C_{eq}} \tag{28}$$

the boundary condition becomes

$$\frac{\partial \overline{C}}{\partial \overline{n}} = -K_w\overline{C}. \tag{29}$$

Replacement of $\overline{C}$ in equations (22) and (23) produce the identical set of equations to be solved as in the previous two sections. The fact that the physical process is assumed isothermal is reasonable in the initial time period and for a solid with a large thermal capacity. An important extention of this problem has been presented by Onischak and Gidaspow [10] where they show that an engineering pseudo-equilibrium value may be used instead of the true equilibrium value. This pseudo-equilibrium value is reproducible and almost independent of time and flow rate.

OVERALL PARAMETERS—FULLY DEVELOPED SOLUTION

The mixing cup concentration or temperature at any axial distance is defined by

$$U \,.\, T_m \,.\, A = \iint u_z \,.\, T \,.\, \mathrm{d}x\,\mathrm{d}y. \tag{30}$$

In terms of the previously defined dimensionless velocity,

$$\overline{T}_m = \iint g(\xi, \eta)\, \overline{T}(\zeta, \xi, \eta) \,.\, \mathrm{d}\xi\,\mathrm{d}\eta. \tag{31}$$

The local average heat transfer coefficient $h_z(z)$ defined at a given z but an average over the cross-section is defined by the simple overall balance

$$A \,.\, U \,.\, \rho C_P \frac{\mathrm{d}T_m}{\mathrm{d}z} = -h_z\overline{P}\left(T_m - \frac{1}{\overline{P}}\oint T_w\,\mathrm{d}_s\right) \tag{32}$$

where the last term in this equation is an average wall temperature over the boundary at any ζ. In terms of the previous dimensionless variables,

$$Nu_z = -\frac{1}{4}\left(\frac{D_h}{2a}\right)^2 \frac{(\mathrm{d}\overline{T}_m/\mathrm{d}\zeta)}{(\overline{T}_m - \overline{\overline{T}}_w)}, \tag{33}$$

where

$$Nu_z = \frac{h_z D_h}{k} \tag{34}$$

and $\overline{\overline{T}}_w$ represents the last term in equation (32).

An overall local heat transfer coefficient $h_{oz}(z)$ which is defined in terms of the solid temperature is also useful to the engineer. It is defined as

$$AU\rho C_P \frac{\mathrm{d}T_m}{\mathrm{d}z} = -h_{oz}\overline{P}(T_m - T_{si}). \tag{35}$$

In terms of dimensionless variables

$$Nu_{oz} = -\frac{1}{4}\left(\frac{D_h}{2a}\right)^2 \frac{\mathrm{d}\overline{T}_m/\mathrm{d}\xi}{\overline{T}_m}. \tag{36}$$

The Nusselt number, Nu_{oz}, is more useful than Nu_z to the engineer, but Nu_z is normally reported in the literature because it varies much less with boundary conditions and therefore may be reported more accurately. Also, the values of Nu_z approach the constant flux Nusselt numbers as the Biot number approaches zero. One may be obtained from the other because a relationship may be derived between them in terms of the boundary conditions by

integrating the partial differential equation in the gas over the cross section and using Green's theorem in the plane to obtain

$$\rho C_P \frac{\mathrm{d}}{\mathrm{d}z}\iint u_z \,.\, T \,.\, \mathrm{d}x\,\mathrm{d}y = k\iint\left(\frac{\partial^2 T}{\partial x^2}+\frac{\partial^2 T}{\partial y^2}\right)\mathrm{d}x\,\mathrm{d}y \tag{37}$$

$$= k\oint \nabla T \,.\, n\,\mathrm{d}s = k\bar{P}\frac{\overline{\mathrm{d}T}}{\mathrm{d}n}. \tag{38}$$

Integration of the boundary conditions over the boundary yields

$$k\frac{\overline{\mathrm{d}T}}{\mathrm{d}n} = -h_w \cdot \frac{1}{\bar{P}}\oint (T_w - T_{si})\,\mathrm{d}s \tag{39}$$

or by definition

$$k\frac{\overline{\mathrm{d}T}}{\mathrm{d}n} = -h_z\left(T_m - \frac{1}{P}\oint T_w\,\mathrm{d}s\right). \tag{40}$$

The definition of h_z in equation (40) may be seen to be coincident with the definition of equation (32) by substitution of equations (30) and (40) into equation (38).

Then Nu_z may be related to Nu_{oz} by combining equations (30), (32), (39) and (40)

$$\rho C_P U A\frac{\mathrm{d}T_m}{\mathrm{d}z} = -\bar{P}\frac{1}{(1/h_z + 1/h_w)}(T_m - T_{si}). \tag{41}$$

Comparison of equation (41) with (35) yields an expression for h_{oz}. In terms of Nusselt numbers, the desired relation is

$$\frac{1}{Nu_{oz}} = \frac{1}{Nu_z} + \frac{1}{Bi(D_h/2a)}. \tag{42}$$

Therefore, it is seen that only Nu_z need be reported even for this unusual geometry. When the resistance at the wall is negligible ($Bi = \infty$), then

$$Nu_{oz} = Nu_z.$$

The existence of a fully-developed solution to this problem further reduces the amount of results which must be reported. The form of the fully developed solution can be obtained by separation of variables.

Let $\overline{T} = Z(\zeta)G(\xi,\eta)$ and separate variables to obtain:

$$\frac{\mathrm{d}Z_k}{\mathrm{d}\zeta} + \beta^2 Z_k = 0 \tag{43}$$

$$\gamma^2\frac{\partial^2 G_k}{\partial\bar{\xi}^2} + \frac{\partial^2 G_k}{\partial\eta^2} + \beta_k^2 \,.\, g \,.\, G_k = 0 \tag{44}$$

$$\left.\frac{\partial G_k}{\partial\bar{n}}\right|_w = -BiG_k|_w. \tag{45}$$

Orthogonality may be demonstrated by combining two solutions G_k and G_j and integrating in the usual way [11] to obtain

$$\iint [G_k\nabla^2 G_j - G_j\nabla^2 G_k + (\beta_j^2 - \beta_k^2)\,gG_j \,.\, G_k]\,\mathrm{d}\bar{\xi}\,\mathrm{d}\eta = 0, \tag{46}$$

where $\bar{\xi} = \xi/\gamma$.

Green's theorem states:

$$\iint (G_k\nabla^2 G_j + \nabla G_k \,.\, \nabla G_j)\,\mathrm{d}\bar{\xi}\,\mathrm{d}\eta = \oint G_k\nabla G_j \,.\, n\,\mathrm{d}s. \tag{47}$$

Equation (46) may be recast as

$$\oint (G_k\nabla G_j - G_j\nabla G_k)\,.\,\bar{n}\,\mathrm{d}s = (\beta_k^2 - \beta_j^2)\iint gG_j \,.\, G_k\,\mathrm{d}\bar{\xi}\,\mathrm{d}\eta. \tag{48}$$

Boundary conditions substituted in equation (48) then require for $k \neq j$

$$\iint gG_jG_k\,\mathrm{d}\bar{\xi}\,\mathrm{d}\eta = 0,$$

which is the condition of orthogonality. The general solution to the problem may be written as:

$$\overline{T} = \sum_{n=1}^{\infty} A_n \exp(-\beta_n^2\zeta)\,G_n(\xi,\eta) \tag{49}$$

where

$$A_n = \frac{\iint g \,.\, G_n\,\mathrm{d}\bar{\xi}\,\mathrm{d}\eta}{\iint g \,.\, G_n^2\,\mathrm{d}\bar{\xi}\,\mathrm{d}\eta}. \tag{50}$$

Since g is positive within the region, β_n^2 are all real and positive and the eigenfunctions form a complete set. If the series converges, the first

term of the solution must become the dominant term for increasing ξ.

The quantities of interest approach the following fully developed forms:

$$\bar{T} = A_1 \exp(-\beta_1^2 \zeta)\, G_1(\xi, \eta) \tag{51}$$

$$\bar{T}_m = (A_1 \cdot \iint g \cdot G_1) \cdot \exp(-\beta_1^2 \xi) \tag{52}$$

$$Nu_{oz} = \frac{1}{4}\left(\frac{D_h}{2a}\right)^2 \beta_1^2 \tag{53}$$

Therefore the numerical solution need only be continued until $\bar{T}_0$ and $\bar{T}_m$ become straight lines on semilog paper and until Nu_{oz} (or Nu_z) become a constant.

SOLUTION BY FINITE DIFFERENCES

Since the equation for the velocity profile does not involve the temperature function, the velocity profile may be determined independently of the temperature profile. Then, the temperature profile, and consequently the total heat transfer, can be solved for after the velocity profile is substituted into the energy equation.

A pseudo-unsteady state technique was used to solve for the velocity profile. This technique consists of adding an unsteady state term to equation (5) which becomes

$$\frac{\partial f}{\partial \tau} = 1 + \frac{\partial^2 f}{\partial \eta^2} + \gamma^2 \frac{\partial^2 f}{\partial \xi}. \tag{54}$$

The steady state solution to this equation is the solution to equation (5). Equation (54) was treated by a second order finite difference approximation and iterated until it converged to a steady state answer. The usual implicit molecule was used to solve this equation.

On the grid next to the lower boundary, the explicit method may be used since no additional stability restriction will be added. However, on the irregular wall, a completely implicit molecule was used. Use of an explicit molecule on the irregular boundary would introduce a very restrictive stability requirement on the entire calculation.

The energy equation with boundary condition given in equation (24) and initial condition given in equation (23) were solved by the method of Dufort and Frankel [12]. The three-dimensional analogy of Dufort and Frankel's three grid finite difference scheme is:

$$\begin{aligned}\bar{T}(I+1, J, K)\{g(J, K) + 2R(1+\gamma^2)\} &= \bar{T}(I-1, J, K)\{g(J, K) - 2R(1+\gamma^2)\} \\ &+ 2\gamma^2 R\{\bar{T}(I, J+1, K) + \bar{T}(I, J-1, K)\} \\ &+ 2R\{\bar{T}(I, J, K+1) + \bar{T}(I, J, K-1)\}.\end{aligned} \tag{55}$$

The fact that the velocity is very small near the wall could cause severe stability restrictions. Use of this method alleviates this problem.

Since the boundary condition on the wall involves the derivative at the wall, a satisfactory expression which is of the same order of error as the interior molecule must be used. A five point expansion is satisfactory. This is obtained by expressing the normal derivative in terms of its components.

Following Greenspan [13] a six point Taylor series expansion was used to represent the normal derivative:

$$\frac{\partial \bar{T}}{\partial n} = \frac{\partial \bar{T}}{\partial \eta} \cdot \sin\lambda + \frac{\partial \bar{T}}{\partial \xi} \cdot \cos\lambda = \sum_{i=0}^{5} \alpha_i \bar{T}_i, \tag{56}$$

where λ is the angle shown in Fig. 3.

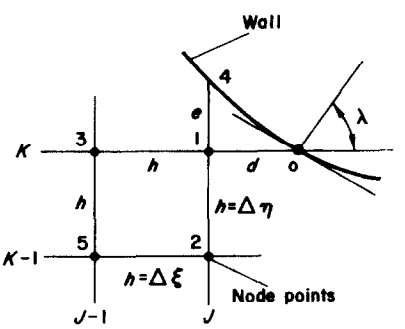

FIG. 3. Irregular boundary geometry.

A Taylor series expansion for points $\bar{T}_0$ through $\bar{T}_5$ about point 0 is substituted into the right hand side of equation (56). Like derivatives are matched and the resulting equations are solved simultaneously for α_0–α_5. The values of α_i used for the molecule about point 0 are given below:

$$\alpha_0 = \frac{(h + 2d)\gamma \cos \lambda}{d(h + d)}$$

$$\alpha_2 = \frac{-(hd + eh + de) \sin \lambda}{h^2(e + h)}$$

$$\alpha_4 = \frac{h}{e(e + h)} \sin \lambda$$

$$\alpha_5 = \frac{d}{h^2} \sin \lambda \qquad (57)$$

$$\alpha_3 = \frac{hd\gamma \cos \lambda - d(d + h) \sin \lambda}{h^2(d + h)}$$

$$\alpha_1 = \frac{(hde - h^2 d + d^2 e)\sin \lambda - he\gamma(h + d)\cos \lambda}{h^2 de}$$

By symmetry, these coefficients can be used to obtain the proper coefficients for a similar equation about point 4. In order that no stability restrictions be introduced at the boundary, equation (56) is written in a completely implicit manner about points 4 and 0. Furthermore, the equation about point 1 is also implicit. These three equations are solved simultaneously for the temperatures at points 1, 0, and 4. There are locations on the irregular boundary where more than three simultaneous equations are needed and, in general, the smaller the grid size chosen, the greater the number of simultaneous equations at any boundary point.

Along the lower boundary, equation (57) is also used; however, it simplifies to a three point molecule because of the regular geometry shown in Fig. 4. An explicit molecule was sufficient at point 1 so $\bar{T}$ at point 0 can be calculated directly.

An additional complication occurs due to the shape of the corner of the duct, which turned out to be a formidable problem. The corner geometry, with a grid overlay is illustrated in Fig. 5. The small portion of the corner including points 1–7 had to be removed from the analysis since no suitable molecules are available for these. As the grid size is made smaller, the size of the region removed decreases, and in the limit it becomes negligible. Notice that in Fig. 5, no points in the region are lost. In this corner region, points 8–14 were solved for simultaneously with the implicit methods previously mentioned.

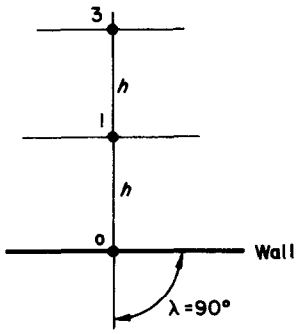

FIG. 4. Lower boundary geometry.

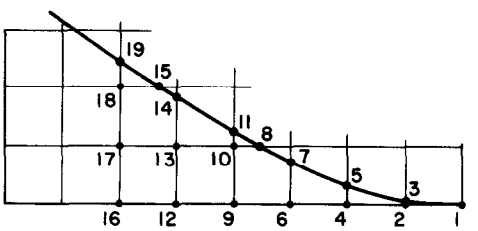

FIG. 5. Corner geometry.

RESULTS

Accuracy of numerical procedure

In any finite difference investigation, it is necessary to test the convergence and stability of the results. In the absence of any theoretical solutions, convergence and stability may be tested by obtaining results for different grid sizes. Consistency of the finite difference equations for the velocity profile is guaranteed and the truncation error is of the order

$$E_T = O(\Delta\tau) + O(\Delta\xi)^2 + O(\Delta\eta)^2$$

Specification of R yields

$$E_T = O(\Delta\xi)^2.$$

The truncation of the energy equation is also of the same order with the same definition of R.

The results for a grid size of $\frac{1}{32}$ compared to that of $\frac{1}{16}$ on the same iteration agreed in the third decimal place for the velocity at any point in the region. In order to compare this technique with published results, the velocity program was simplified to the case of a triangular duct and friction factors were calculated and compared to published values. For an aspect ratio of one, our calculated friction factor was 13·26; Sparrow [14] reported a value of 13·18 for this same case.

Although all reported results for the temperature problem were obtained with a $\Delta\xi = \frac{1}{32}$ grid size, a program with a $\Delta\xi = \frac{1}{16}$ grid size was also written for convergence testing. Due to the nature of the equations which are solved along the boundary, a separate program had to be written for each grid size so that only these grid sizes were investigated. The temperature at any grid point agreed to the third significant decimal again. A second means of checking the results from the two temperature programs was to use a very large Biot number for the flux problem and compare the average internal temperature to the program with constant temperature wall. The infinite Nusselt numbers agreed in the third significant figure and as the Biot number increases, the average interior temperatures approached each other.

Furthermore, the two Nusselt numbers in equations (33) and (36) were calculated and checked against each other with use of equation (42). The comparison of these is shown in Table 1 for selected values. It is seen that difference in these values decrease with increasing Biot number.

CALCULATED RESULTS

Table 2 gives the values of $F \cdot N_{Re}$ calculated by equation (8) and entrance length from equation (10) for various aspect ratios. These are plotted in Fig. 6 with values for the triangular duct. For a given aspect ratio, the area of the triangular and sinusoidal duct are equal and the hydraulic radii differ by 2·5 per cent at an aspect ratio of one. From Fig. 6 it is evident that the pressure drop is lower for the sinu-

Table 1. Comparison of accuracy of $\frac{1}{16}$ and $\frac{1}{32}$ grid sizes, aspect ratio of one

Bi	Nu	Nu_0	$\frac{1}{Nu_0}$	$\frac{1}{Nu} + \frac{1}{Bi(D_h/2a)}$	$\frac{1/Nu + 1/Bi.(D_h/2a)}{1/Nu_0}$
			$\Delta x = \frac{1}{16}$		
0·01	1·183	0·00714	140	124·8	0·89
0·1	1·380	0·0668	14·9	13·12	0·88
1·0	1·590	0·4972	2·01	1·86	0·925
10·0	1·972	1·567	0·640	0·633	0·995
100·0	2·077	2·023	0·494	0·493	0·999
			$\Delta x = \frac{1}{32}$		
0·01	1·415	0·00737	135	124·7	0·91
0·1	1·308	0·0703	14·2	13·16	0·925
1·0	1·524	0·5085	1·97	1·89	0·962
10·0	1·974	1·579	0·644	0·630	0·980
100·0	2·093	2·039	0·491	0·490	0·999

Table 2. Calculated friction factor and entrance length

$\gamma = \frac{a}{b}$	$F \cdot N_{Re}$	$\bar{u}$	$\frac{Z_e}{D_h N_{Re}}$	K	$\frac{U_m}{U}$	$\frac{D_h}{2a}$
0·25	9·68	0·0490	0·0613	2·168	2·355	0·978
0·50	10·05	0·0341	0·0555	2·011	2·290	0·931
1·00	11·14	0·0294	0·0465	1·809	2·209	0·809
1·50	12·07	0·0200	0·0426	1·750	2·193	0·696
2·00	12·95	0·0141	0·0401	1·743	2·196	0·604
3·00	13·89	0·0080	0·0398	1·813	2·241	0·472

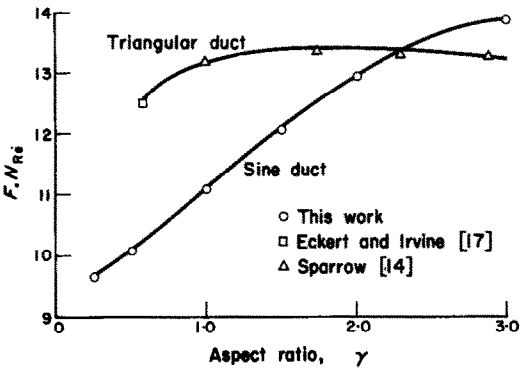

FIG. 6. Friction factor for sinusoidal duct.

soidal duct than for the triangular duct. This statement holds even if the pressure drop for the two ducts are compared at equal flow rates. The data of Howard [1] is compared in Fig. 7

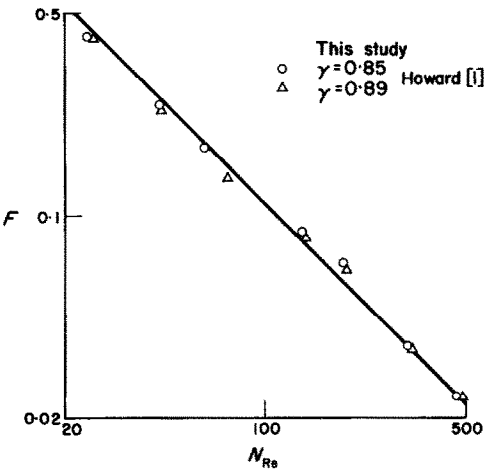

FIG. 7. Comparison of measured and calculated friction factors.

and shows a maximum deviation of 6·5 per cent over our calculated values of $F \cdot N_{Re}$. As the aspect ratio increases, the friction factors for the triangular and sinusoidal duct approach each other. The entrance length is shown in Fig. 8 and shows the entrance length for the sinusoidal duct is longer than that of the triangular duct. Figure 9 shows the fully developed velocity profile for the half-duct

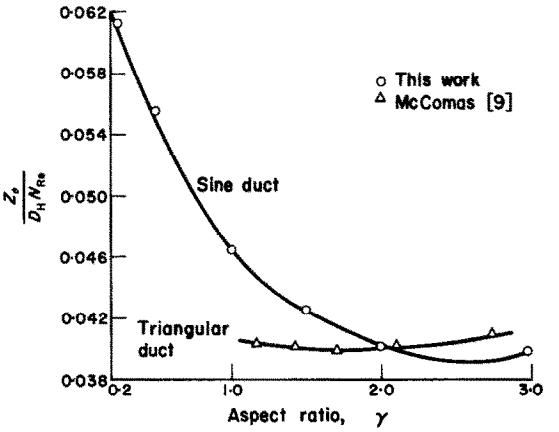

FIG. 8. Entrance length for sinusoidal duct.

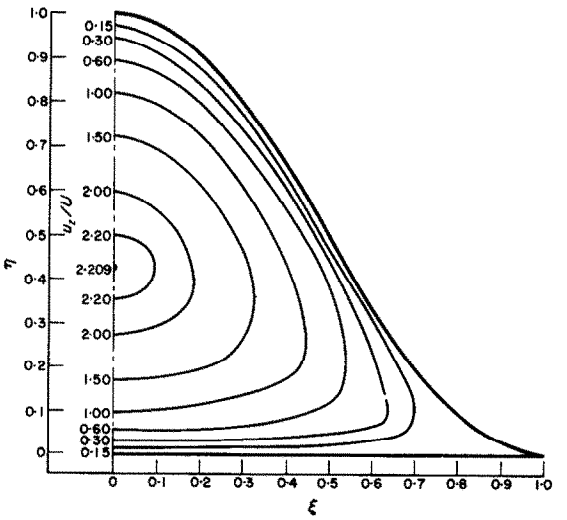

FIG. 9. Fully developed velocity profile for an aspect ratio of one.

with an aspect ratio of one. The isoclines are lines of constant u_z/U. It is interesting to note that the maximum velocity occurs closer to the center than those of the triangular duct [14] for similar aspect ratios.

For Howard's data, the ducts had aspect ratios of 0·85 and 0·89. For these aspect ratios, the entrance length parameter was $Z_e/D_hN_{Re} = 0{\cdot}048$. His data was taken over a range of dimensionless lengths corresponding to:

$$7{\cdot}4 > \frac{L}{N_{Re}D_h} > 0{\cdot}37.$$

This indicates that the duct length was at least 8 times the hydrodynamic entrance length.

On the other hand, Kays and London [15] reported FN_{Re} to be between 18 and 19 for a sinusoidal duct with an aspect ratio of 2·77. The calculated value of FN_{Re} was 13·8. The calculated entrance length was $Z_e/D_hN_{Re} = 0{\cdot}0392$. These data were taken over a dimensionless length range of:

$$0{\cdot}020 < \frac{L}{D_hN_{Re}} < 0{\cdot}041$$

This indicates that all the data were taken in the hydrodynamic entrance region and hence our results should not and do not agree with theirs.

Figure 10 shows the limiting Nusselt numbers as a function of aspect ratio for the case of constant wall temperature. This corresponds to the boundary condition given in equation (19)

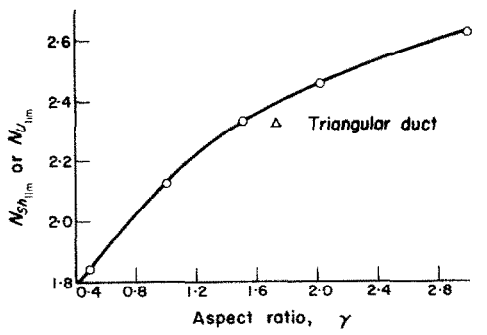

FIG. 10. Nu_{1m} for constant temperature wall vs. aspect ratio.

where $Bi = \infty$. For the case of an equilateral triangle, the value of this Nusselt number is 2·35 [16]. This corresponds to an aspect ratio of about 1·73 and from Fig. 10 the limiting Nusselt number is approximately 2·37 for the sinusoidal duct. Howard presents Nusselt numbers for aspect ratios between 0·85 and 0·89 as shown in Table 3. The mean value of Nu is

Table 3. Data of Howard converted to units of the study

Friction factor			Nusselt number		
F	N_{Re}	$F.N_{Re}$	j	N_{Re}	$Nu = j.N_{Re}.N_{Pe}^{\frac{1}{3}}$
Metal: brass $\gamma = 0{\cdot}85$					
0·0231	496	11·45	0·00524	490	2·25
0·0595	185	11·0	0·00830	305	1·97
0·1747	61·1	10·68	0·0143	182	2·28
0·420	24·1	10·12	0·0248	120	2·61
				Calculated value	2·045
Metal: stainless steel $\gamma = 0{\cdot}89$					
0·0231	496	11·50	0·00641	311	1·77
0·0580	188	10·90	0·0119	183	1·93
0·1389	73·5	10·20	0·0181	122	1·96
0·410	24·6	10·10	0·0301	72·5	1·94
			0·0455	42·6	1·72
			0·0726	24·3	1·56
				Calculated value	2·070

Note: Calculated Peclet number in air is 0·671.

1·99 and the variance about this value is small. The calculated values of Nu for the constant wall temperature case corresponding to this aspect ratio range is betwen 2·05 and 2·06. Since Howard took heat transfer data in stainless steel and brass ducts, the assumption of a constant temperature wall should be good in light of the high thermal conductivity of the metal.

Figure 11 shows how the dimensionless temperature in the duct varies as the wall resistance changes. These solutions correspond to the boundary condition given in equation (19) and were obtained for a single aspect ratio, $\gamma = 1{\cdot}0$. This plot can be used with equation (36) to obtain Nu_{oz} as a function of distance and equation (42) to obtain Nu_z. Table 4 gives the values of the limiting Nusselt numbers for the variable wall resistance cases. It should be noted

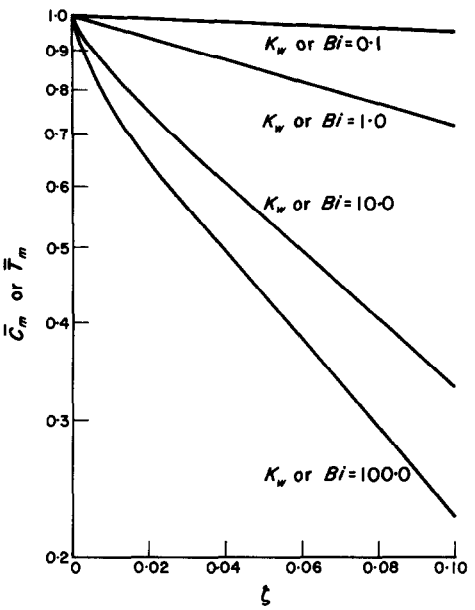

FIG. 11. Temperature vs. distance for an aspect ratio of one.

Table 4. Limiting Nusselt numbers for an aspect ratio of one

K_w or Bi	$Nu_{\lim}$
0·010	1·415
0·100	1·308
1·00	1·524
10·0	1·974
100·0	2·096
∞	2·12

that the limiting values of Nu were in every case lower than those of the constant temperature wall. Reported values of the limiting Nusselt numbers for finite Biot numbers for other types of geometries are usually higher than those of the constant temperature wall [16]. Thus, it appears that the sine duct is a rather unique heat transfer geometry.

CONCLUSIONS

One might expect that the geometry in Fig. 1 could be represented by something between a circle and flat plate configuration. However the friction factors and Nusselt numbers for these geometries are much higher than those of the sinusoidal profile. The friction factors for the triangular geometries, shown in Fig. 6, is within 10 per cent of those for the sinusoidal duct at high aspect ratios (greater than 1·5), but at lower aspect ratios, they differ considerably. This indicates that the sinusoidal duct is more efficient than the triangular duct since the hydraulic diameters of these two configurations are very close. The Nusselt numbers calculated for constant temperature wall agree well with data previously published. In general the limiting Nusselt numbers for the sine duct are lower than for other geometries. However, at an aspect ratio of 1·7, the Nusselt number for this geometry is higher than that of a triangular duct.

These seemingly inconsistent results arise from the corner of the sinusoidal duct where there is a relatively large dead space. This is reflected in the large entrance lengths found for this configuration as compared with other geometries.

REFERENCES

1. C. P. HOWARD, *J. Engng Pwr* **87**, 72 (1965).
2. G. L. LOCKE, Heat transfer and flow friction characteristics of porous solids, TR-No. 10, Dept. of Mech. Engr., Stanford Univ., Stanford, Calif. (1950).
3. T. E. W. SCHUMANN, *J. Franklin Inst.* **208**, 405 (1929).
4. J. R. MONDT, *Int. Heat Transfer Conf.* Boulder, Col. Paper No. 73, Proc. ASME (1961).
5. L. A. CRESWICK, *Ind. Math.* **8**, 61 (1957).
6. R. W. LYCZKOWSKI, C. W. SOLBRIG and D. GIDASPOW, Forced convective heat transfer—general case of wall resistances and peripheral condition, Submitted to SIAM Journal on Applied Mathematics.
7. J. G. KNUDSEN and D. L. KATZ, *Fluid Dynamics and Heat Transfer*. McGraw-Hill, New York (1958).
8. C. W. SOLBRIG, Ph.D. Thesis, Ill. Inst. of Tech., Chicago, Ill. (1966).
9. S. T. MCCOMAS, *J. Basic Engng* **89**, 847 (1967).
10. M. ONISCHAK and D. GIDASPOW, *Can. J. Chem. Engng* (1968). In print.
11. C. C. BARTLETT and B. NOBLE, *Appl. Sci. Res.* **B9**, 403 (1963).
12. E. C. DUFORT and S. P. FRANKEL, *Math. Tables Aids Comput.* **7**, 135 (1953).
13. D. GREENSPAN, *Introductory Analysis of Elliptic Boundary Value Problems*, pp. 39–42. Harper & Row, New York (1956).
14. E. M. SPARROW, *A.I.Ch.E. Jl* **8**, 599 (1962).
15. W. KAYS and A. L. LONDON, *Compact Heat Exchangers*, p. 195. McGraw-Hill, New York (1964).

16. W. A. KAYS and A. L. LONDON, *Compact Heat Exchangers*, p. 103. McGraw-Hill, New York (1964).

17. E. R. G. ECKERT and T. F. IRVINE, JR., *Fifth Midwest Conf. Fluid Mechanics*, p. 41. University of Mich. Press, Ann Arbor, Mich. (1957).

ETUDE ANALYTIQUE DES COEFFICIENTS DE TRANSPORT DE CHALEUR OU DE MASSE ET DE FROTTEMENT DANS UN ÉCHANGEUR DE CHALEUR OU DE MASSE À TUYAUX ONDULÉS

Résumé—Les paramètres pour prévoir le transport de masse et de chaleur sont disponibles facilement pour l'écoulement dans des tuyaux circulaires ou plats avec un grand nombre de conditions aux limites. Cependant, les frontières des conduits trouvés habituellement dans les régénérateurs, les échangeurs de chaleur tornants, les échangeurs de masse tournants, etc, ne sont forcément ni circulaires ni à plaques parallèles. Un échangeur très ordinaire constitué de nombreux conduits ressemble à la vue en bout de plusieurs couches de carton ondulé. La frontière de la section droite normale à l'écoulement d'un de ces conduits peut être représentée par une courbe sinusoïdale allant de $-\pi$ à π formant la portion supérieure du conduit et d'une plaque plane étendue entre $-\pi$ et π pour former la portion inférieure de la frontière.

Cet article présente les coefficients de frottement et les nombres de Nusselt (ou les nombres de Sherwood) calculés pour cette géométrie avec plusieurs allongements et nombres de Biot (ou vitesses de réaction à la paroi). Ces résultats sont en bon accord avec les données expérimentales très limitées signalées dans la littérature. Puisque ces données sont limitées, cette analyse fournit une information supplémentaire de prévision sur une géométrie très importante du point de vue du transport de chaleur et de masse. Les résultats obtenus ne pourraient pas être estimés d'un façon adéquate à partir de ceux d'une géométrie circulaire ou d'un tuyau plat parce que les coins du tuyau sinusoïdal correspondent à une géométrie proprement différente. Les résultats diffèrent aussi considérablement de ceux d'un tuyau triangulaire. Un résultat remarquable pour la géométrie sinusoïdale est le comportement du nombre de Nusselt qui décroît lorsque le nombre de Bior décroît.

ANALYTISCHE UNTERSUCHUNG DES WÄRME- ODER STOFFÜBERGANGS UND DES REIBUNGSKOEFFIZIENTEN IN EINEM WELLROHR-WÄRME- ODER STOFFÜBERTRAGER

Zusammenfassung—Für Strömungen in Rohren und zwischen parallelen Platten unter verschiedenen Randbedingungen lassen sich die, für Auslegungsrechnungen benötigten Wärme- und Stoffaustausch-Parameter leicht auffinden. Indessen handelt es sich bei den Strömungsquerschnitten von Regeneratoren, rotierenden Wärme- und Stoffaustauschern etc. aus technischen Gründen meist um andere, als die oben beschriebenen Geometrien.

Eine häufig zu findende Austauschbauart mit vielen Strömungskanälen zeigt eine Querschnittsform, ähnlich einer Schichtung aus mehreren Lagen Wellpappe. Die Berandung eines dieser, senkrecht zur Strömungsrichtung geschnittenen Kanäle kann durch eine Sinuskurve für die Kanaloberseite und eine ebene Platte für die Kanalunterseite—jeweils mit den Intervallgrenzen $-\pi$ und $+\pi$—dargestellt werden.

Die vorliegende Arbeit zeigt berechnete Reibungsbeiwerte und Nusselt-Zahlen (oder Sherwood-Zahlen) für diese Geometrie bei mehreren Abmessungsverhältnissen und Biot-Zahlen (oder Wandreaktionsraten).

Diese Ergebnisse stimmen recht gut mit den sehr spärlichen, in der Literatur zu findenden experimentellen Daten überein. Da die Literatur sehr wenig Daten enthält, bietet diese Untersuchung zusätzliche Information für die Auslegung einer sehr wichtigen Wärme- und Stoffaustauscher-Geometrie. Es war nicht möglich, die erhaltenen Resultate zufriedenstellend aus den Ergebnissen für das Kreisrohr oder den ebenen Spalt herzuleiten, da aufgrund der Ecken im Kanal mit teilweise sinusförmiger Berandung eine wesentlich verschiedene Geometrie vorliegt. Die Ergebnisse zeigen auch beträchtliche Abweichungen von denen eines Dreieck-Kanals. Ein ungewöhnliches Ergebnis bei der Sinusgeometrie ist das Verhalten der Nusselt-Zahl; diese nimmt ab mit fallender Biot-Zahl.

АНАЛИТИЧЕСКОЕ ИССЛЕДОВАНИЕ ТЕПЛО- И МАССООБМЕНА И КОЭФФИЦИЕНТА ТРЕНИЯ В ТЕПЛО- И МАССООБМЕННИКАХ ТИПА ИЗОГНУТЫХ ТРУБОК

Аннотация—Для условий течения жидкости в круглых и плоских каналах имеются параметры при различных граничных условиях для расчета тепло-и массопереноса каналов. Однако проточные каналы в регенераторах, вращающихся теплообменниках, вращающихся массообменных аппаратах и т.д. по необходимости являются не круглюми и не плоскими. Вид с торца такого устройства, состоящего из многочисленных каналов, напоминает несколько слоев гофрированного картона. Границу перпендикулярного потоку сечения одного из этих ходов можно представить синусной кривой—π–π,

образующей верхнюю часть канала, и плоской пластиной, расположенной между— π и π и образующей нижнюю часть границы.

В данной статье представлены рассчитанные коэффициенты трения и критерия Нуссельта (или Шервуда) для нескольких видовых отношений и критериев Био (или скорости реакции на стенке). Эти результаты хорошо согласуются с имеющимися в литературе оченв ограниченными экспериментальными данными. Поскольку имеющиеся в литературе данные ограничены, настоящий анализ дает дополнительную информацию по расчету очень важных форм тепло-и массообмена поверхностей. Получнные результаты не могли быть удовлетворительно оценены по результатам для круглых или плоских каналов, потому что из-за углов в синусоидальном канале получается совершенно отличная геометрия. Результаты также значительно отличаются от полученных в треугольном канале. Необычным результатом синосоидальной геометрии явилось поведение критерия Нуссельта. Критерий уменьшается с уменьшением критерия Био.